Proceedings of the
International Conference on Mechanical Engineering 2005
(ICME2005) 28- 30 December 2005, Dhaka, Bangladesh

ICME05-FL-25

FLOW CHARACTERISTICS OF TWO NON-PARALLEL STREAMS BEHIND A FINITE THICKNESS BASE

Mohammad Ali, M.Quamrul Islam and A. K. M. Monjur Morshed

Department of Mechanical Engineering, Bangladesh University of Engineerinh & Technology, Dhaka-1000, Bangladesh.

ABSTRACT

The objectives of this study are to observe the mixing of subsonic hydrogen flow with supersonic airflow, characteristic phenomena of the flowfield, mixing efficiency and flame holding capability of a supersonic combustor. Two non-parallel streams are considered for this study where merging angle is varied. This numerical study has been performed by solving Two-Dimensional Navier-Stokes equations. An explicit Harten-Yee Non-MUSCL Modified -Flux-Type TVD (Total Variational Diminishing) scheme has been used to solve the system of equations, and a zero-equation algebraic turbulence model proposed by Baldwin and Lomax has been used to calculate the eddy viscosity coefficient. To delineate the purely fluid dynamic effects, the flow has been treated as non-reacting. It has been seen that recirculation and penetration of hydrogen play an important role to enhance mixing. The area of recirculation decreases with the increase of merging angle but mixing efficiency increases. The recirculation regions and several shocks such as expansion shock, recompression shock and reattachment shock in the flowfield are evident.

Keywords: Scramjet engine, TVD scheme, Thickness base, Merging angle.

1. INTRODUCTION

Mixing process plays a vital role in flowfield of many engineering applications e.g. combustion chambers, pre-mixers for gas turbine combustors, chemical lasers, propulsion systems and flow reactors. In supersonic combustor, the flow speeds are very high and mixing of injectant with mainstream is difficult due to their short residence time. A considerable number of researches, not only by experiment but also by numerical methods, have been carried out on mixing and combustion of fuel with supersonic air stream for the last three decades.

In recent development of efficient Supersonic Combustion Ramjet (Scramjet) engines and advanced airspace propulsion system, there is renewed interest in the study of turbulent mixing layers. The turbulent mixing layer, which forms at the interface between two uniform streams of different velocity, develops through two succes- sively distinct regions. Unfortunately, Liou et al [1] showed that the growth rate of mixing layer in two supersonic streams is considerably smaller than that of two subsonic streams. Brown & Roshko [2] showed that the spreading rate of supersonic mixing layer decreased drastically with increasing of free stream Mach number. Azim and Islam [3] showed that the mixing layers decreased in growth with increasing velocity ratio and mixing layers from non-parallel merging streams (18°) were found to have higher growth in the near-field than those from parallel merging streams. Recirculation in flowfield is very important factor for mixing in supersonic combustor. Recirculation formed behind the base or step can enhance mixing and flame holding capability.

There exist several methods of fuel injection in the supersonic air stream. Perpendicular injection causes rapid fuel-air mixing whereas parallel injection is used when slow process is desired, especially at lower speed of space vehicles. In parallel injection, mixing occurred by molecular diffusion at the interface of two flows [4~5]. The mixing layer from non-parallel merging streams has higher growth than those from parallel merging streams.

Hydrogen is well known as the most suitable fuel for propulsion systems. Because of the high speed of the air stream, a reasonable length is needed for the combustor. So it is difficult to perform the experimental study under the supersonic combustion because of high cost. Therefore, the numerical research is quite important. There is no available information about the effect of air-hydrogen non-parallel streams behind a base, which is shown in this paper.

2. GOVERNING EQUATIONS

The flowfield is governed by the unsteady, two-dimensional Navier-Stokes equation neglecting body forces and heat source terms, along with species continuity equations and an energy equation. With the conservation-law form, these equations can be expressed by

$$\frac{\partial U}{\partial t}+\frac{\partial F}{\partial x}+\frac{\partial G}{\partial y}=\frac{\partial F_v}{\partial x}+\frac{\partial G_v}{\partial y} \qquad (1)$$

Where

$$U=\begin{pmatrix}\rho\\ \rho u\\ \rho v\\ E\\ \rho_i\end{pmatrix},\quad F=\begin{pmatrix}\rho u\\ \rho u^2+p\\ \rho uv\\ (E+p)u\\ \rho_i u\end{pmatrix},\quad G=\begin{pmatrix}\rho v\\ \rho uv\\ \rho v^2+p\\ (E+p)v\\ \rho_i v\end{pmatrix}$$

$$F_v=\begin{pmatrix}0\\ \sigma_x\\ \tau_{xy}\\ \sigma_x u+\tau_{xy}v+q_x\\ \bullet\\ m_x\end{pmatrix},\quad G_v=\begin{pmatrix}0\\ \tau_{xy}\\ \sigma_y\\ \tau_{yx}u+\sigma_y v+q_y\\ \bullet\\ m_y\end{pmatrix}$$

The pressure is calculated from the equation of state for ideal gas expressed as

$$p=\sum_{i=1}^{ns}\rho_i R_i T = \sum_{i=1}^{ns}\rho_i\frac{R}{W_i}T$$

The total energy E can be expressed by

$$E=\sum_{i=1}^{ns}\rho_i h_i-\sum_{i=1}^{ns}\rho_i\frac{R}{W_i}T+\frac{\rho}{2}\left(u^2+v^2\right)$$

$$=\sum_{i=1}^{ns}\rho_i C_{pi}T-\sum_{i=1}^{ns}\rho_i\frac{R}{W_i}T+\frac{\rho}{2}\left(u^2+v^2\right)$$

σ, τ and q may be obtained from the following equations

$$\sigma_x=\lambda\left(\frac{\partial u}{\partial x}+\frac{\partial v}{\partial y}\right)+2\mu\left(\frac{\partial u}{\partial x}\right)$$

$$\sigma_y=\lambda\left(\frac{\partial u}{\partial x}+\frac{\partial v}{\partial y}\right)+2\mu\left(\frac{\partial v}{\partial y}\right)$$

$$\tau_{xy}=\tau_{yx}=\mu\left(\frac{\partial u}{\partial y}+\frac{\partial v}{\partial x}\right),\quad \lambda=\frac{2}{3}\mu$$

$$q_x=-k\frac{\partial T}{\partial x}-\sum_{i=1}^{ns}D_{iml}h_i\frac{\partial Y_i}{\partial x}$$

$$q_y=-k\frac{\partial T}{\partial y}-\sum_{i=1}^{ns}D_{iml}h_i\frac{\partial Y_i}{\partial y}$$

3. NUMERICAL SCHEME AND GRID SYSTEM

The system of governing equation is solved, using an explicit Harten-Yee Non-MUSCL Modified-flux-type TVD scheme [6]. The two-dimensional, rectangular physical coordinate system (x, y) is transformed into the computational coordinate system (ξ, η) in order to solve the problem on uniform grids. After applying the transformation procedure, Eq. (1) can be expressed as:

$$\frac{\partial \hat{U}}{\partial t}+\frac{\partial \hat{F}}{\partial \xi}+\frac{\partial \hat{G}}{\partial \eta}=\frac{\partial \hat{F}_v}{\partial \xi}+\frac{\partial \hat{G}_v}{\partial \eta} \qquad (2)$$

where

$$\hat{U}=J^{-1}U,\quad \hat{F}=J^{-1}(\xi_x F+\xi_y G)$$

$$\hat{G}=J^{-1}(\eta_x F+\eta_y G)$$

$$\hat{F}_v=J^{-1}(\xi_x F_v+\xi_y G_v)$$

$$\hat{G}_v=J^{-1}(\eta_x F_v+\eta_y G_v)$$

The grid Jacobian J and metric terms are,

$$J^{-1}=x_\xi y_\eta-x_\eta y_\xi$$

$$\xi_x=Jy_\eta,\ \xi_y=-Jx_\eta,\quad \eta_x=-Jy_\xi,\ \eta_y=J_\xi$$

The grid system consists of 142 nodes in the longitudinal direction and 101 nodes in the transverse direction. The grid points around the left wall and behind the base are clustered to ensure high resolution in near-wake and shear-layer regions.

4. RESULTS AND DISCUSSION

The geometric configuration of the calculation domain and the inlet condition of two non-parallel streams is shown in Fig. 1.

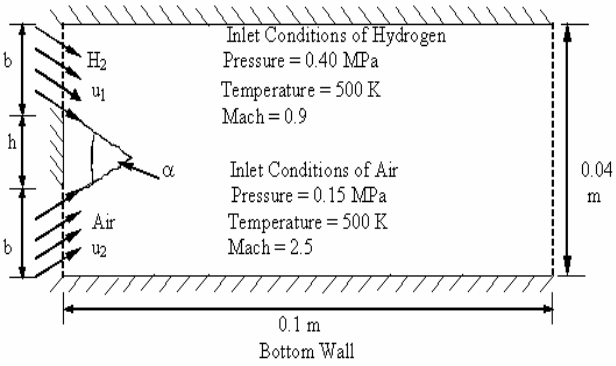

Fig 1. Schematic with numerical parameters for varying the merging angle of air and hydrogen streams (Merging angle, α=10^0, 20^0, 30^0, 40^0 & 50^0; Base thickness, h = 0.01 m; Inlet width, b = 0.015 m)

Some features of this kind of flow field are shown in Fig. 2, which shows different shocks and boundary layer arrangements.

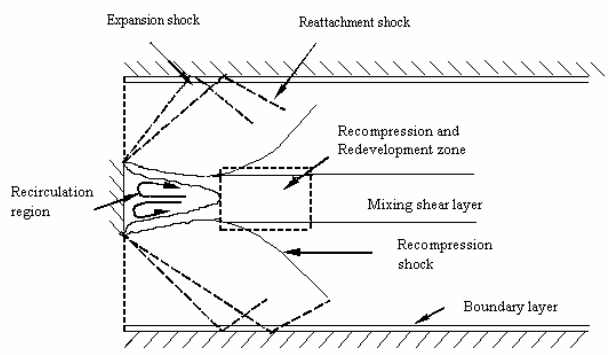

Fig 2. Flow field characteristics generated by two non-parallel streams behind a thickness base

Figures 3 (a-e) show velocity vectors of the physical model, where the flows expand sharply around the base corner and produce a separation region behind the base. Direction of arrow indicates flow direction and arrow length indicates the magnitude of velocity. Both hydrogen and air flows move to each other and strike behind base at about 0.02 m from the bottom wall. After striking, hydrogen flow deflects upward and airflow deflects downward. Again these flows strike the upper and lower walls and then reflect. There is a pair of recirculation region moving in opposite direction behind the base. The upper recirculation rotates clockwise while the lower recirculation rotates counter clockwise. The maximum negative velocity in recirculation is lower than that of the inlet velocity of hydrogen or air. The flows expand sharply around the base and higher interaction occurs with the low velocity regions of both shear layers. For two recirculations moving in opposite directions, hydrogen mixes with air and provides a mixing region. Due to interaction between two streams, the velocity of the stream is slowed down and both hydrogen and air enter in recirculation regions. Again by diffusion and convection, hydrogen enters into the recirculation region and mixes with air. So recirculation plays a vital role on the mixing. The shear layer mixing regions spread with longitudinal distance until impingement occurs, where the recirculation region ends (no negative longitudinal velocity) and recovery of the wake deficit begins. The turbulent mixing occurs throughout the recompression and reattachment region and far away of downstream. The impingement point distance from the left wall decreases with the increase of merging angle, which indicates smaller recirculation zones. For example, for Case-1 and 2, impingements occur at approximately x = 0.018 and 0.013 m from left wall respectively. So the area of recirculation zone decreases with the increase of merging angle.

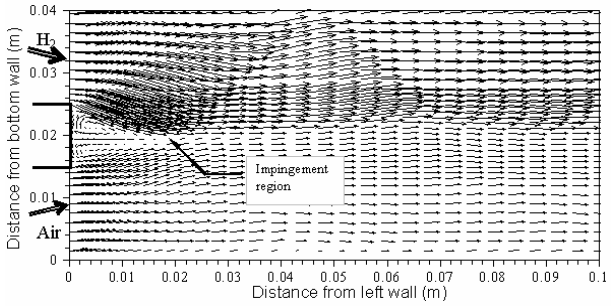

Fig 3(a). Velocity vector of two streams; Case-1 ($\alpha = 10^0$)

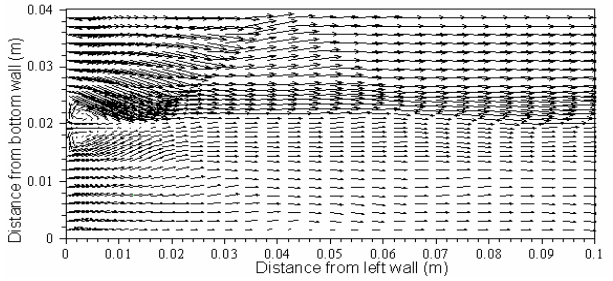

Fig 3(b). Velocity vector of two streams; Case-2 ($\alpha = 20^0$)

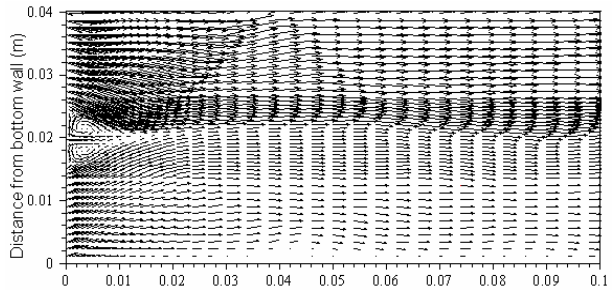

Fig 3(c). Velocity vector of two streams; Case-3 ($\alpha = 30^0$)

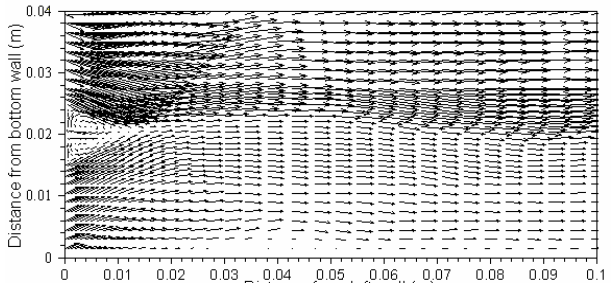

Fig 3(d). Velocity vector of two streams; Case-4 ($\alpha = 40^0$)

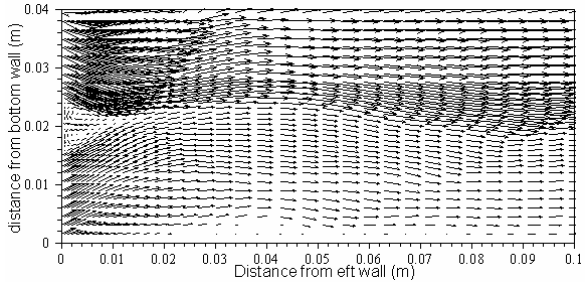

Fig 3(e). Velocity vector of two streams; Case-5 ($\alpha = 50^0$)

To see the strength of recirculation and magnitude of the negative velocity, longitudinal velocity profiles, non-dimensionalized by the x-direction velocity (u_1=1530 m/s) of hydrogen are shown in Fig.4 Only case-1 and case-4 are discussed for these types of profiles. The dashed line at x value represents the lengthwise location of the traverse and the $u/u_1 = 0$ plane for that set of data. The series of profiles indicate the large negative velocities occurring in recirculating region and the recovery of the velocity defect with downstream distance.

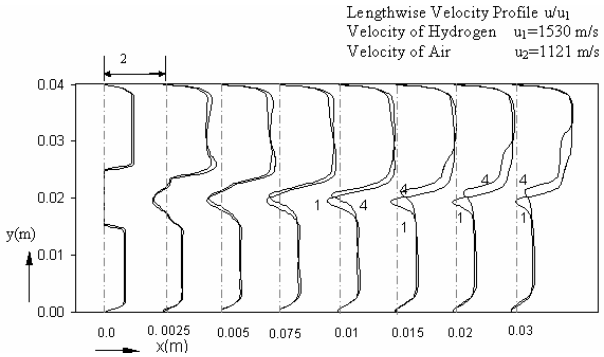

Fig 4. Lengthwise velocity profiles of the flow field showing the near-wake region; (for Case-1 and case-4).

Figures 5 (a~e) show mole fraction contours of hydrogen in the flow field. The concentration ratio contour allows the growth of the mixing layer clearly. As can be seen in Figs. 5 (a~e), the mixing layers grow along the flow direction. Penetration and mixing of hydrogen with air can occur by means of (i) strong interaction occurred with the low velocity regions of both shear layers (ii) turbulence and convection due to recirculation and velocity of the flow and (iii) molecular diffusion. For all cases (1~5), mole fraction contours show that the mixing shear-layer is relatively narrow in width at interaction region of hydrogen and air. The width of the mixing layer is defined as the length from the location of 5% to that of 100% concentration ratio of hydrogen. The width of mixing layer at far downstream increases with merging angle. As the lower flow is air and upper flow is hydrogen, the significant density gradient exists at the interface of two flows and hydrogen mixes with air in one interface. In this work, there is a pair of recirculation regions behind the base as discussed earlier. Out of two recirculation regions, the upper recirculation contains high concentration of hydrogen (mole fraction is about 0.85~0.95) due to the convection and strong expanded flow of hydrogen. On the other hand, in lower recirculation region, hydrogen mixes with air by convection and diffusion processes. This region contains better proportion of hydrogen and air (mole fraction is about 0.65 ~ 0.85), which is capable of burning.

Longer recirculation zone containing better stoichiometric mixture strength results in a longer residence time of flow and leads to a more stable flame. Flame holding capability is better for case-1 than that of other cases as it can produce larger and elongated recirculations, where the lower recirculation contains better proportion of hydrogen and oxygen.

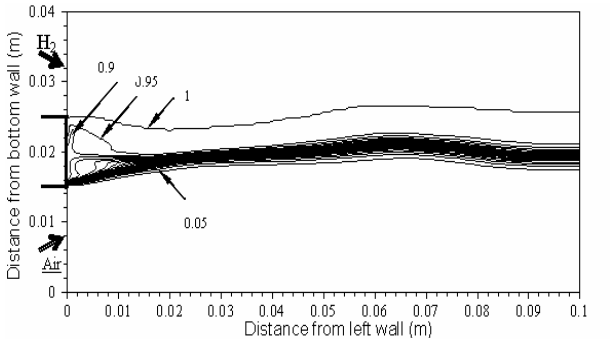

Fig 5(a). Mole fraction contour of hydrogen, φ (0.05,1.0,0.05); Case-1 ($\alpha = 10^0$).

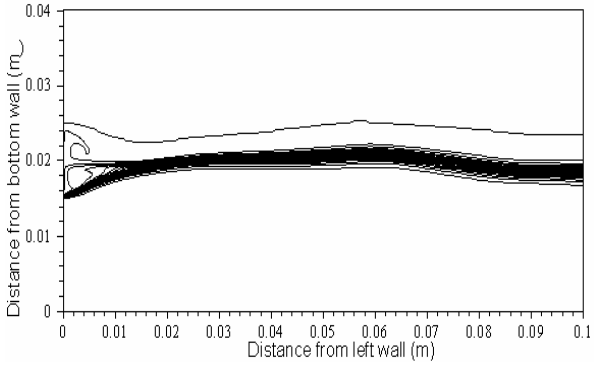

Fig 5(b). Mole fraction contour of hydrogen, φ (0.05,1.0,0.05); Case-2 ($\alpha = 20^0$).

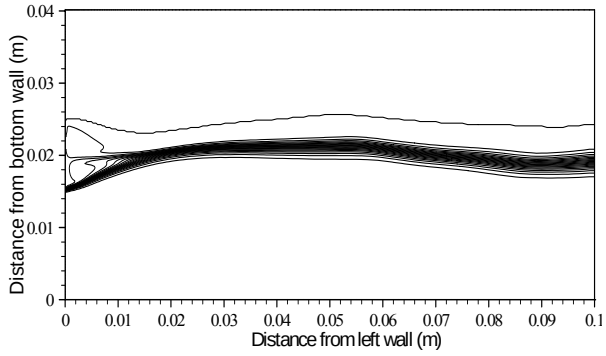

Fig 5(c). Mole fraction contour of hydrogen, φ (0.05,1.0,0.05); Case-3 ($\alpha = 30^0$).

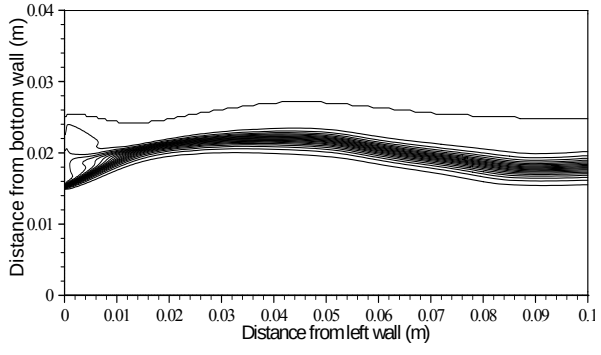

Fig 5(d). Mole fraction contour of hydrogen, φ (0.05,1.0,0.05); Case-4 ($\alpha = 40^0$).

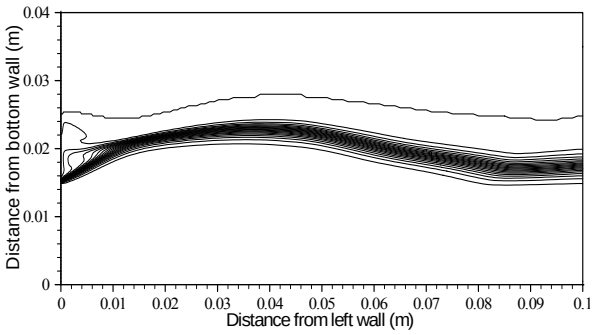

Fig 5(e). Mole fraction contour of hydrogen, φ (0.05,1.0,0.05); Case-5 ($\alpha = 50^0$).

However, The larger recirculation region does not mean higher mixing efficiency. Figure 6 shows mixing efficiency along the length of physical model for different cases.

Mathematically, the mixing efficiency is defined by

$$\eta_m = \frac{\int_A \left(\int_H \rho \vec{u} \; d\vec{A} \right) / \phi'}{\dot{m}_H / \Phi}$$

Where,

A = arbitrary section plane

$\int_H$ = local mass fraction of hydrogen

ρ= total density

$\vec{u}$ = velocity vector

$d\vec{A}$= small area normal to velocity vector

$\dot{m}_H$ = total mass flux of hydrogen

$$\phi' = \text{local equivalence ratio} = \begin{cases} 0.25 & \phi' < 0.25 \\ \phi' & \phi' \geq 0.25 \end{cases}$$

$$\Phi = \text{global equivalence ratio} = \begin{cases} 0.25 & \Phi < 0.25 \\ \Phi & \Phi \geq 0.25 \end{cases}$$

Figure 6 shows that for all cases the mixing efficiency increases sharply just behind the base due to strong interaction around the base corner and recirculations. In recirculation region, the increment of mixing is high and then it is slow. The increasing rate of mixing is very slow at far downstream because of the supersonic nature of flow. By comparing all the cases, it is observed that the mixing efficiency in recirculation regions as well as the overall mixing efficiency at the outflow boundary increases with increasing merging angle up to 40^0 and then decreases sharply. The effect of merging angle on overall mixing efficiency is shown Fig.7 for cases (1~5).

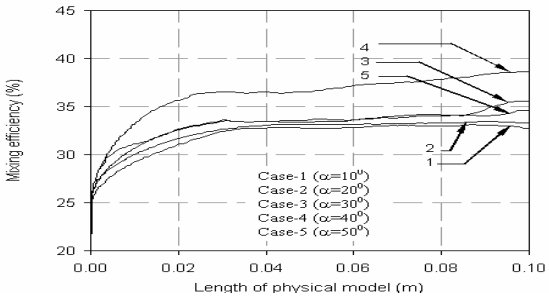

Fig 6. Mixing efficiency along the length of physical model.

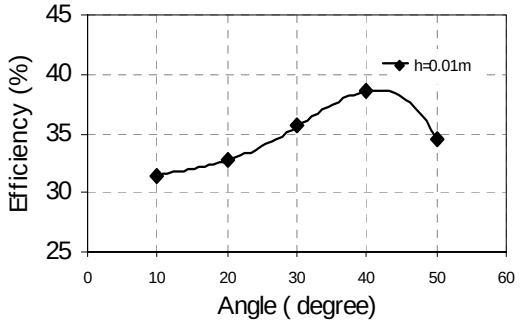

Fig 7. Variation of mixing efficiency vs. merging angles.

The pressure at different region such as the recirculation, recompression, redevelopment and reattachment process can be clearly seen by the profile of static pressure along a centerline physical domain shown in Fig. 8

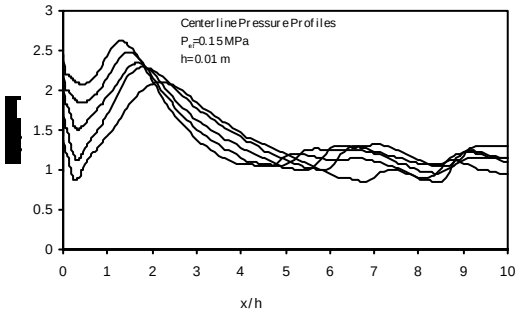

Fig 8. Centerline pressure profiles of the flow field

The static pressure is non-dimensionalized by the inlet pressure of air (0.15 MPa) and the streamwise distance is non-dimensionalized by the value of thickness base height (h= 0.01 m). Figure 8 indicates the lower pressure existing in the recirculating region just downstream of the base and the strong pressure rise, which occurs during the recompression and impingement processes. When the merging angle is small, the pressure in recirculation region decreases sharply. However, pressure in reciculation region tends to become constant with increase of merging angle. Figure 8 also shows that the base pressure and the maximum pressure in recompression and redevelopment region increase with merging angle. Low pressure indicates higher diffusion

and higher diffusion means better mixing in recirculation region. The distance of the highest value of $P/P_{ref.}$ decreases with the increase of merging angle, which indicates that recompression region moves toward the left wall. Far away from the left wall, the centerline pressure profile shows low pressure and wavy nature with small amplitude.

5. CONCLUSIONS

The present study has been conducted with the variation of merging angle of two non-parallel streams. It is found that interaction between air and hydrogen flows increases with merging angle but the area of recirculation region decreases. The increasing rate of mixing efficiency behind the base is high and then it is very slow. For 40^0 merging angle, the mixing efficiency is high but the flame holding capability is comparatively lower. For high merging angle (50^0), both the mixing efficiency and flame holding capability are low. In this study, hydrogen can mix with airflow in one region (one interface) along the shear layer. The area of the mixing regions can not increase with the increase of merging angle. So a configuration will be found out so that mixing can occur in two or more interfaces. Zero-equation model is mathematically simple because it requires no additional field equation and contains only a few modeling constants. The two main limitations are (i) it is not suitable for complex separated flows and (ii) it has no account of convection and diffusion of turbulence. So two-equation turbulence model is suggested to overcome these difficulties. This is a two-dimensional case. Three-dimensional calculations are required for real flow field.

6. NOMENCLATURE

Symbol	Meaning	Unit
B	inlet height of the stream	(m)
E	total energy	(J/m^3)
F	flux vector in x-direction	
$\hat{F}$	transformed flux vector in -direction	
G	flux vector in y-direction	
$\hat{G}$	transformed flux vector in η-direction	
h	finite-thickness base width	(m)
J	transformation Jacobian	
p	pressure	(Pa)
R	universal gas constant,	J/(kg.mol.K)
t	physical time	(Second)
T	temperature	(K)
u	horizontal velocity	(m/s)
U	vector of conservative variables	
$\hat{U}$	transformed vector of conservative variables	
v	vertical velocity	(m/s)
W	molecular weight of species	(gm/mol)
α	merging angle	(Degree)
q_c	energy flux by conduction	(W/m^2)
ξ	transformed coordinate in horizontal direction	(-)
η	transformed coordinate in vertical direction	(-)
ρ	mass density	(kg/m^3)
σ	normal stress	(Pa)
τ	shear stress	(Pa)
μ	coefficient of dynamic viscosity	(kg/m.s)
δ	boundary layer thickness	(m)

7. REFERENCES

1. Liou, T-. M., Lien, W-. Y., and Hwang, P-. W., 1995, "Compressibility Effects and Mixing Enhancement in Turbulent Free Shear Flows", AIAA Journal, Vol. 33, No. 12, pp. 2332-2338
2. Brown, G. L., and Roshko, A., 1974, "On Density Effects and Large Structure Turbulent Mixing Layers", Journal of Fluid Mech. Vol. 64, Part. 4, pp. 775-816.
3. Azim, M. A., and Islam A. K. M. S., 2003, "Plane Mixing Layers From Parallel and Non-Parallel Merging of Two Streams", Experiments in fluids, Vol. 34, pp. 220-226.
4. Umeda, Y., and Fujiwara, T., 1995 "Physics of Methane Combustion in Mixing Shear Layer", Trans. Japan Soc. Aero. Space Sci., Vol. 38, No. 121, , pp. 265-281.
5. Gerlinger, P., Algermissen, J., and Bruggemann, D., 1996,"Numerical Simulation of Mixing for Turbulent Slot Injection", AIAA Journal, Vol. 34, No. 1, , pp. 73-78.
6. Yee,H.C. ,1989 "A class of High-Resolution Explict and Implicit Shock-Computing Methods", NASA TM 101088.
7. Tabejamaat, S., Ju, Y., and Niioka, T., 1997, "Numerical Simulation of Secondary Combustion of Hydrogen Injected from Preburner into Supersonic Airflow", AIAA Journal, Vol. 35, No. 9, pp. 1441-1447.